JGR Earth Surface

RESEARCH ARTICLE
10.1029/2020JF005808

Site Dependence of Fluvial Incision Rate Scaling With Timescale

Ron Nativ[1,2,3] and Jens M. Turowski[3]

[1]Department of Earth and Environmental Sciences, Ben-Gurion University of the Negev, Beer Sheva, Israel, [2]Institute of Earth and Environmental Science, University of Potsdam, Potsdam, Germany, [3]GFZ German Research Centre for Geosciences, Telegrafenberg, Potsdam, Potsdam, Germany

Key Points:
- Fluvial bedrock incision rates decrease with the timescale over which they are averaged
- Among the examined models, a power law model with a site-dependent exponent is consistent with 26 previously published field data sets
- An empirical equation is proposed to remove the Sadler effect and make incision rates measured at different timescales comparable

Supporting Information:
- Supporting Information S1

Correspondence to:
R. Nativ,
ronnat@post.bgu.ac.il

Citation:
Nativ, R., & Turowski, J. M. (2020). Site dependence of fluvial incision rate scaling with timescale. *Journal of Geophysical Research: Earth Surface*, *125*, e2020JF005808. https://doi.org/10.1029/2020JF005808

Received 28 JUL 2020
Accepted 5 OCT 2020
Accepted article online 13 OCT 2020

Abstract Global measurements of incision rate typically show a negative scaling with the timescale over which they were averaged, a phenomenon referred to as the "Sadler effect." This time dependency is thought to result from hiatus periods between incision phases, which leads to a power law scaling of incision rate with timescale. Alternatively, the "Sadler effect" has been argued to be a consequence of the mobility of the modern river bed, where the timescale dependency of incision rates arises from a bias due to the choice of the reference system. In this case, incision rates should be independent of the timescale, provided that the correct reference system is chosen. It is unclear which model best explains the "Sadler effect," and, if a timescale dependency exists, which mathematical formulation can be used to describe it. Here, we present a compilation of 581 bedrock incision rates from 34 studies, averaged over timescales ranging from single floods to millions of years. We constrain the functional relationship between incision rate and timescale and show that time-independent incision rate is inconsistent with the global data. Using a power law dependence, a single constant power is inconsistent with the distribution of observed exponents. Therefore, the scaling exponent is site dependent. Consequently, incision rates measured over contrasting timescales cannot be meaningfully compared between different field sites without properly considering the "Sadler effect." We explore the controls on the variable exponents and propose an empirical equation to correct observed incision rates for their timescale dependency.

Plain Language Summary The rate at which rivers cut into their own bed (incision) typically decreases with the age of past river surfaces used to infer it. This phenomenon, previously described for numerous geological processes, has been traditionally attributed to be a result of an unsteady incision process over the time of investigation. Alternatively, it has been argued that it is a consequence of a measurement bias that can occur when the modern river bed is used as a reference point. To test which of these contrasting hypotheses is valid, we designed specific tests for the competing models, yielding statistical criteria that can be used against actual data. We compiled data on river incision from 34 papers and compared them to the tests. A bias due to the choice of the modern river bed as reference point cannot explain the observations. Instead, we find a site-specific dependence of incision on timescale. Thus, when comparing incision rates measured at different sites, time dependency needs to be corrected for. Using the field data, we offer a simple empirical equation that can be utilized for such a correction.

1. Introduction

Fluvial incision into bedrock can occur rapidly, with meters of incision during a single flood event, but more commonly it is a slow process that unfolds over geological timescales of thousands and millions of years. Incision rate is a key process governing mountain denudation, channel geometry and hillslope-channel coupling (e.g., Whipple, 2004). Constraining incision rates in bedrock rivers is of primary interest in fluvial geomorphology, as the tectonic and climatic signatures of a specific location in a specific time period can be assessed. Process-based models, such as the stream power model for erosion, have been used to infer signals of rock uplift (e.g., DiBiase et al., 2010; Wobus et al., 2006), climate (e.g., Ferrier et al., 2013), and lithology (Duvall et al., 2004). For these purposes, field data are required that often include measurements of fluvial incision rates. When comparing different field settings, incision rates that integrate over different timescales are frequently placed in the same space to constrain regional climatic and uplift histories, or to study controls on channel morphology and dynamics (e.g., Harel et al., 2016). However, like other process rates such as subsidence, uplift, and sediment accumulation, channel incision rates are dependent on the timescale of

the measurement (Finnegan et al., 2014; Gallen et al., 2015; Gardner et al., 1987; Mills, 2000). This phenomenon is generally referred to as the "Sadler effect" (Sadler, 1981). Sadler (1981) showed that a substantial fraction in the variance of sediment accumulation rates in stratigraphic columns over ~11 magnitudes is due to a correlation with timescale.

Numerous methods are available for constraining fluvial incision rates. Calculations over short timescales (days, weeks, months and years; e.g., Hartshorn et al., 2002; Turowski et al., 2008) can be achieved using different methods and techniques, repeated topographic surveys or comparison to natural or artificial benchmarks (Turowski & Cook, 2017). However, for the purposes of interpreting longer-term climatic and tectonic signals from incision rates, a suit of radiogenic isotopes are used to date markers which record past river bed locations. Such markers include strath terraces (e.g., Burbank et al., 1996; Harkins et al., 2007), incised lava plateaus (e.g., Dethier, 2001; Gani et al., 2007), caves (e.g., G. M. Stock et al., 2005) and alluvial fill above strath terraces (e.g., Pazzaglia & Brandon, 2001). The elevation difference between the marker and the current streambed is then divided by the marker age to yield an estimate of the average incision rate.

In this paper, we address the question of the time dependence in fluvial bedrock incision. We compiled a data set of 581 measurements of bedrock incision rates in fluvial environments. We utilize this data set to achieve the following objectives: (1) to test whether previously published incision rate data are time dependent or free from time dependence and (2) to establish an empirical relation between incision and timescale for practical usage, in the case that rates are dependent on timescale. We start by reviewing the "Sadler effect" and the different mechanisms that were proposed to explain it.

1.1. The "Sadler Effect": Theory and Mechanisms

Barrell (1917) asserted that discontinuities in sediment columns exist in all eras, but are more frequent in old sequences. According to him, "the lost intervals" increase "with more distant eras". Sadler (1981) presented a comprehensive compilation of sediment accumulation rates and thoroughly discussed the possible mechanisms to explain their observed time dependence. The term "Sadler effect" is attributed to this work. Many other rate processes, nonetheless, have shown to be dependent on the time period over which they are averaged (e.g., Gardner et al., 1987). In essence, the "Sadler effect" means a scaling of a physical length Z, for example an erosion or incision depth, with the timescale of the measurement T, described by the following power law

$$Z = aT^{\gamma} \tag{1}$$

where a and γ are constants. The rate of change in length, I is achieved by dividing Z by T

$$I = \frac{Z}{T} = aT^{\gamma - 1} \tag{2}$$

The dependency of rate processes on timescale has been traditionally modeled by treating it as a nonsteady process that incorporates multiple periods of hiatus of different time lengths, during which the process is delayed (Sadler, 1981; Sadler et al., 1999; Schumer & Jerolmack, 2009). For a steady process over time, $\gamma = 1$ and the rate I is independent of timescale. However, values of $0 < \gamma < 1$ are commonly observed when fitting Equation 2 to field data (e.g., Pelletier, 2007; Pelletier & Turcotte, 1997), which indicates a decrease in process rate for larger timescales.

Using field data to constrain the relationship between the process rate and timescale, Gardner et al. (1987) found the scaling exponent $\gamma = 0.82$ for landscape denudation data, whereas Mills (2000) found $\gamma = 0.39$ for bedrock incision rates. Ganti et al. (2016) found γ values that range 0.29 to 0.89 for glaciated landscapes and posed the question whether this is caused by hiatus periods in erosion or whether erosion rates increased over time toward the present. Finnegan et al. (2014) explicitly assessed the existence of timescale-dependent incision rate in bedrock channels, using data from 14 different sites, and found that the relation between γ and timescale is independent of tectonic activity, which was defined as a region that experiences tectonically driven uplift. In their compilation, γ varied between 0.5 and 1.5 for different sites, with a value of 0.8 for the entire data set.

The observed scaling between incision rate and timescale that occurs due to the "Sadler effect" potentially masks real trends of incision rate over time. For example, it may be consequential to an extended ongoing debate that has examined the premise that climate and erosion rates are coupled in a complex, arguably bidirectional way. Whether the late Cenozoic uplift is an effect of cooling climate or vice versa (Molnar & England, 1990), it has been suggested that despite the reasoning that climate shifted to cooler temperatures, weathering rate, denudation and erosion have essentially been constant over the Cenozoic (Willenbring & Jerolmack, 2016; Willenbring & Von Blanckenburg, 2010). Seemingly, this is inconsistent with the wide range of processes that exhibit increasing rates toward the present (e.g., Finnegan et al., 2014; Ganti et al., 2016; Sadler et al., 1999), and may imply a different mechanism. However, if the scaling of the rate with timescale is apparent, as the "Sadler effect" signifies, then it is crucial to unravel its mechanism in order to make progress toward differentiation of real from apparent rates.

Most existing theoretical models predict a power law scaling of sediment accumulation rate with timescale. Plotnick (1986) introduced a fractal model, according to which a hiatus gap G is introduced in the middle of an accumulated sediment column. The parameter $G = \frac{T_H}{T_{tot}}$ describes the hiatus period (T_H) as a fraction of the total timescale considered (T_{tot}). For example, consider a sediment column of 1,000 m that was deposited over a period of $T_{tot} = 100$ kyr. The average deposition rate is 1 m/1,000 yr. If G is 1/2, there is a hiatus of one half of the total deposit period ($T_H = GT_{tot}$=50 kyr) in the middle of the sediment column, creating two 500 m sediment columns with a total deposit time of 25 kyr and an average deposition rate of 40 m/1,000 yr each. Each pile is then subdivided again, into two 250 m piles, with a hiatus of 25 kyr. As this process is continued, it produces a negative power law dependence of accumulation rate on timescale, such as Equation 2, where the power is given in terms of G by

$$\gamma = -\frac{\log(1-G)}{\log\left[\frac{(1-G)}{2}\right]}) \tag{3}$$

An outcome of this model is that the power γ may bear information about the hiatus in sedimentation in a specific study site, because G can be retrieved numerically if γ is known. A one-dimensional Brownian motion-based model of stratigraphic columns (Sadler & Strauss, 1990; Strauss & Sadler, 1989) was also used to explain the Sadler effect. This model predicts

$$Z \propto T^{0.5} \tag{4}$$

Pelletier and Turcotte (1997) introduced an extended version of a random walk model with sediment mobilization described by a diffusion equation. Their model predicts

$$Z \propto T^{0.25} \tag{5}$$

Schumer and Jerolmack (2009) exploited a Continuous Time Random Walk (CTRW) that describes sediment accumulation as a stochastic process. The CTRW is a discrete random walk process that equates the surface location to the sum of all discrete accumulation events ("jumps"), which are considered instantaneous and constant in the model. Between these jumps, there are time durations where sediment accumulation does not exist ("waiting times" or "hiatus"). The hiatus are drawn from a probability density function $\chi(t)$. Schumer and Jerolmack (2009) explored the dependency of Z on T through different $\chi(t)$ characteristics using the solution to a CTRW (Metzler & Klafter, 2000). They considered two distinct cases, each describing the nature of the hiatus probability function's right-hand tail. In the first case, the tail decays exponentially to 0 with increasing time, and a well-defined, finite mean exists. Then, incision rate I is independent of T

$$\frac{Z}{T} = I = \frac{C}{\mu} \tag{6}$$

Here, C is the observed length (corresponds to Z in Equation 1), and μ is the expected waiting time value $\mu = \int_0^\infty t\chi(t)dt$. In contrast, the second case uses a Pareto distribution $\chi(t) = \kappa t^{-\beta-1}$ with a power law tail, an infinite mean for $\beta \leq 1$ and a finite mean for $\beta > 1$. The scaling of Z with T is nonlinear

$$Z = \frac{I_{LT}}{\Gamma(1-\gamma)} \frac{T^{\gamma}}{\Gamma(1+\gamma)} \tag{7}$$

where I_{LT} is an instantaneous incision rate and $\Gamma(x)$ is the gamma function

$$\Gamma(x) = \int_0^{\infty} y^{x-1} e^{-y} dy \tag{8}$$

Here, y is a dummy variable. The rate is achieved in the same manner as in Equation 2

$$I = \frac{I_{LT}}{\Gamma(1-\gamma)} \frac{T^{\gamma-1}}{\Gamma(1+\gamma)} \tag{9}$$

Equation 9 results in a power law relationship between process rate and timescale with the dependency controlled by the power γ (cf. Pelletier & Turcotte, 1997; Sadler & Strauss, 1990). Using Equation 9, several statements can be made about the exponent γ. First, the gamma function of Equation 8 diverges for a value of 0, that is, the term $\Gamma(1-\gamma)\Gamma(1+\gamma)$ diverges when γ is either -1 or 1 (supporting information Figure S1). Second, for $\gamma > 1$, incision rate increases with timescale (Equation 9). Third, for $-2 < \gamma < -1$, the term $\Gamma(1-\gamma)\Gamma(1+\gamma)$ is negative, and thus, incision rate is negative, which is physically not possible. Using these arguments, the value of γ is expected to be larger than -1 and smaller than 1 (Figure S1).

An alternative mechanistic explanation for the dependency of incision rates on timescale was proposed by Gallen et al. (2015). Instead of a hiatus-induced "Sadler effect," they argued that time dependency can result from a systematic bias in the elevation measurement, which arises when using the modern stream bed as a reference frame for calculations of terrace elevation. This bias is an outcome of the modern channel mobility, which emerges due to aggradation and degradation fluctuations of the modern channel bed relative to the long-term incision rate. In Gallen et al.'s (2015) model, the scaling exponent γ is equal to 1 (cf. Equation 2), provided that any data points related to the modern stream bed are excluded from the analysis. Since the modern stream bed is explicitly not expected to lie on the linear trend, but provides the reference frame for the elevation, a constant t_A needs to be added, accounting for temporary shifts of the modern stream bed elevation. Accordingly, a history of terrace formation forced by a constant incision rate E can be described by a linear relationship between Z and T

$$Z = ET - t_A \tag{10}$$

If only aggradation is considered, t_A should be positive and is the thickness of alluvium above the bedrock; the minus sign reflects that the bedrock elevation Z needs to be lower than that of alluvium. Hereafter, Gallen et al.'s (2015) and Schumer and Jerolmack's (2009) models will be referred to as the "linear" and the "variable exponent power law" models, respectively, whereas Equations 4 and 5 will be referred to as the "constant exponent power law" models (Pelletier & Turcotte, 1997; Sadler & Strauss, 1990; Strauss & Sadler, 1989).

When applied to data from a single site, several of the proposed models (Table 1) yield similar fit qualities, making it hard to differentiate (Figure 1). Thus, to test the models (Table 1), we utilized an artificial data analysis (ADA) approach, concurrently using on data from multiple sites. We pose the following three questions: (i) Can the data be explained with the linear model by Gallen et al. (2015) (Equation 10)? If a nonlinear model is required, (ii) can a single exponent γ explain the data from all the different sites (Pelletier & Turcotte, 1997; Sadler & Strauss, 1990; Strauss & Sadler, 1989)? And (iii) alternatively, if γ is variable for different sites (Schumer & Jerolmack, 2009), what site-specific parameters control it?

2. Methods

2.1. Fluvial Bedrock Incision Data Collection

We compiled direct measurements of fluvial incision rates (Table 2), ignoring studies that report data obtained from methods that integrate over different process domains (e.g., catchment-wide denudation rates by cosmogenic nuclide dating). The reported incision rates were based on a variety of methods, and can be

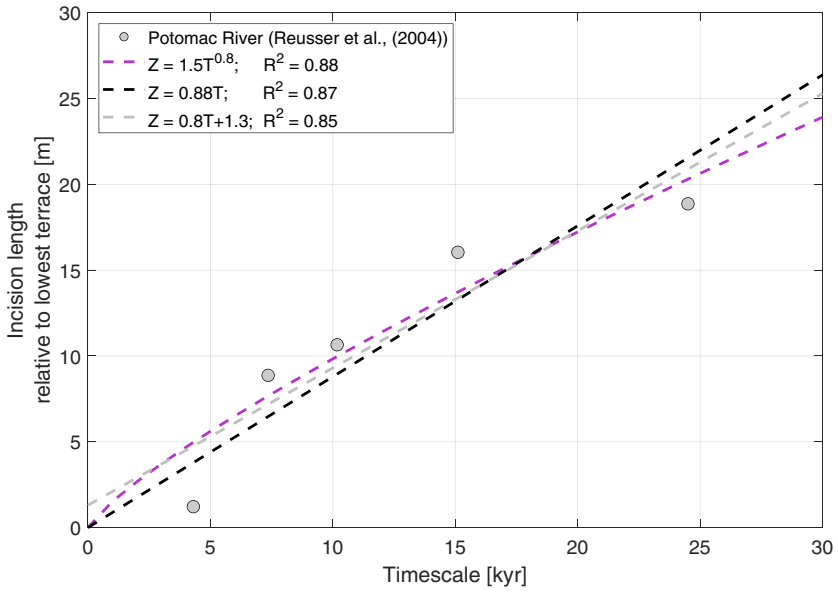

Figure 1. An example of a field-derived data set (Reusser et al., 2004) from the Potomac River. To construct the figure, we calculated the difference between each of the terraces' elevation and age and the lowest terrace, to avoid using the current river bed (Gallen et al., 2015). Curves of power law (Equation 1) and linear (Equation 10) models and their associated R^2 are shown for comparison. The results suggest that the R^2, which is similar among the models, cannot be used as a sole indicator to assess which model best explains the data.

broadly classed into (1) survey methods, measuring bed surface elevation with respect to a fixed marker at different times using, for example, terrestrial laser scanning, or (2) dating methods, obtaining dates from geological or geomorphic markers such as strath terraces (cf. Turowski & Cook, 2017). In the latter case, incision rates were calculated either with respect to a modern marker surface (e.g., the modern river bed) or relative to another dated marker. Using the information given in the papers, we extracted measured incision rates and auxiliary information on location, climate, lithology, tectonic setting, and local fluvial geomorphology (slope, width, drainage area, grain size, characteristic discharge values). The quality and breadth of information given in the papers was highly variable, and mostly only a small subset of the values of interest could be obtained.

For several studies, a number of data points were measured at the same location. For example, surveys with profile gauges include spatially distributed data (e.g., Hartshorn et al., 2002). Likewise, some studies include several measurement periods for the same location (e.g., Cook et al., 2013). In these cases, we included all of the individual data points into the compilation.

Table 1
Previously Published Models Explaining the "Sadler Effect"

	Mechanism	Equation number	Equation	Scaling exponent (γ; Equation 1)	Reference
1	Hiatus in incision	(3)	$Z \propto T^{\gamma}$	$-\frac{\log(1-G)}{\log\left[\frac{(1-G)}{2}\right]}$	Plotnick (1986)
2	Hiatus in incision	(4)	$Z \propto T^{0.5}$	0.5	Strauss and Sadler (1989); Sadler and Strauss (1990)
3	Hiatus in incision	(5)	$Z \propto T^{0.25}$	0.25	Pelletier and Turcotte (1997)
4	Hiatus in incision	(6)	$Z = \frac{C}{\mu}T$	1	Schumer and Jerolmack (2009)
5	Hiatus in incision	(7)	$Z = \frac{I_{LT}}{\Gamma(1-\gamma)}\frac{T^{\gamma}}{\Gamma(1+\gamma)}$	variable	Schumer and Jerolmack (2009)
6	River bed mobility	(10)	$Z = ET - t_A$	1	Gallen et al. (2015)

Journal of Geophysical Research: Earth Surface

10.1029/2020JF005808

Table 2
Performance of Theoretical Models

Data sources used to constrain exponent γ ("model data sets")

	Reference	River	N[a]	Range of measured incision rate (mm yr^{-1})	R^2 ($Z \propto T^{0.5}$)[b]	R^2 ($Z \propto T^{0.25}$)[c]	Best fit γ[d]	Best fit a	R^2	ADA test γ[e]
1	Anthony and Granger (2004)	Western escarpment of the Cumberland Plateau	15	0.016–0.054	0.43	0.41	0.49	41.7	0.68	0.06
2	Antón et al. (2012)	Duero River	18	1.55–17.1	0	0	0.19	35620.3	0.19	−0.25
3	Brocard et al. (2003)	The Buech River	4	0.74–1.33	0.74	0.72	0.73	24.0	0.70	0.53
4	Burbank et al. (1996)	Indus river	7	0.002–0.013	0.51	0.53	0.31	7.2	0.25	0.43
5	Cheng et al. (2002)	Jinshaan Canyon, Yellow River	6	0.16–1.62	0.67	0.59	0.33	2182.1	0.89	0.54
6	Cook et al. (2009)	Glen Canyon, Trachyte Creek	4	0.33–0.53	0.95	0.97	1.73	$5.62\ 10^{-5}$	0.99	1.31
7	Cook et al. (2013)	Da'an River	6	905.7–82124.3	0	0	0.21	6147.8	0.20	0.29
8	Craddock et al. (2010)	Yellow River, China	7	166.7–175675.7	0	0	−0.05	36611.1	0.04	−1.22
9	Crow et al. (2014)	Grand Canyon	36	0.033–3.42	0.08	0.05	0.17	6312.9	0.03	0.13
10	Dortch et al. (2011)	Numerous rivers, India	24	0.024–3.0	0	0	0.12	5906.9	0.03	0.60
11	Gani et al. (2007)	Blue Nile River	12	0.055–0.32	0.22	0.07	0.43	831.9	0.88	0.97
12	Granger et al. (2001)	Mamoth Cave, Green River	28	0.021–0.041	0.70	0.70	0.64	5.3	0.70	0.68
13	Harkins et al. (2007)	Yellow River, China	9	0.54–2.53	0.79	0.81	0.81	15.7	0.73	1.12
14	Johnson et al. (2010)	Swett creek, Mount Hillers, Henry Mountains	4	8.57–771.4	0	0	0.17	173.9	0.05	−0.82
15	Karlstrom et al. (2007)	Grand Canyon	7	0.02–0.11	0.75	0.69	0.45	106.7	0.95	0.58
16	Leland et al. (1998)	Indus River near Nanga Parbat	28	0.65–29.7	0.58	0.55	0.35	4438.6	0.32	0.51
17	Pazzaglia and Brandon (2001)	Clearwater River	61	0.001–1.2	0.04	0.04	0.56	68.6	0.09	0.63
18	Personius (1995)	Numerous rivers, Oregon, USA	31	0.08–5.2	0.49	0.47	1.05	0.20	0.89	0.54
19	Reusser et al. (2004)	Potomac River	9	1.14–4.6	0	0	0.26	2587.2	0.33	0.33
20	Reusser et al. (2006)	Susquehanna River	4	0.03–0.3	0.11	0.23	1.11	0.157	0.96	1.83
21	Schaller et al. (2005)	Liwu River, Taiwan	10	17.6–52.3	0.90	0.87	0.78	191.6	0.90	0.93
22	Seong et al. (2008)	Numerous rivers, North Pakistan	7	2.14–31.9	0	0	−0.05	40380.2	0.08	0.32
23	G. M. Stock et al. (2005)	Southern Sierra Nevada	16	0.015–0.15	0.58	0.60	2.44	$7.83\ 10^{-11}$	0.95	2.16
24	Wegmann and Pazzaglia (2002)	Clearwater River basin	30	0.0003–0.004	0	0.07	1.23	$1.50\ 10^{-4}$	0.30	1.22
25	Wegmann and Pazzaglia (2009)	Bidente River, Italy	6	1–2.2	0.86	0.94	0.88	2.5	0.96	1.05
26	Yanites et al. (2010)	Peikang River, Taiwan	21	0.6–10.2	0.04	0	0.68	54.6	0.60	−0.79
	Average		**15.7**		**0.42**	**0.33**	**0.62**		**0.53**	
	Median		**9.5**		**0.47**	**0.30**	**0.47**		**0.64**	
	Sum		**410**							

Additional data sources used for the empirical Equation 11

	Reference	River	N[a]	Range of measured incision rate (mm yr^{-1})
27	Beer et al. (2017)	Gornera stream, Switzerland	4	0.35–1.55
28	Cyr and Granger (2008)	Esino River, Apennines, Italy	1	0.2
29	Dethier (2001)	Multiple rivers west of the Mississippi River	69	0.02–0.3
30	Hartshorn et al. (2002)	Liwu River, Taiwan	31	1.8–76.3
31	Litchfield and Berryman (2006)	Ten rivers along Central and Eastern North Island	9	1.7–11.8
32	J. D. Stock et al. (2005)	Numerous rivers in the U.S.A and Taiwan	21	0–125
33	Turowski et al. (2008)	Liwu River, Taiwan	22	2.3–124.4
34	Whipple et al. (2000)	Upper Ukak River, Alaska	14	15–110
	Sum		**171**	

[a]Number of data points in the compilation. [b]Model by Strauss and Sadler (1989) and Sadler and Strauss (1990). [c]Model by Pelletier and Turcotte (1997). [d]The power γ is adjusted to maximize the fit, as in the model by Schumer and Jerolmack (2009) [e]The average power was derived using the four-terrace analysis (see text; section 3.2).

To empirically explore the data, we used all compiled data sets from 34 papers. However, for the purpose of validity assessment of models, we used a data set only if it met the following two conditions: (1) The data set contains at least three different data points, and (2) the timescale is not a single value. Using these criteria, we were left with 26 out of 34 usable data sets (hereafter referred to as the "model data sets").

2.2. Evaluating Parameters in the Nonlinear Equations

For each data set, we fitted a power law relation according to Equation 1, using a nonlinear least squares regression. We calculated a and γ (see Equation 1) and computed the coefficient of determination R^2 between each of the data sets and its fitted model. To test the predictive power of the constant exponent power law models, Equations 4 and 5, we fixed the power to 0.5 and 0.25, respectively (Table 1), regressed over the data to determine the prefactor, and recorded the best fit coefficients and R^2. We use the latter to assess model applicability to the different fitted data sets against the empirical relationship with free power γ (Equation 1).

To test whether the linear and the variable exponent power law models, Equations 10 and 7, respectively (Table 1), better describe the data, we designed a test that mimics the development of strath terraces using the assumptions made for the models. In order for the test to be suitable with the field data sets, we recomputed data γ values using the following Monte Carlo approach. Goodness of fit of a regression is dependent on the number of data points. As a result, the regressions on data sets containing different numbers of data points cannot be meaningfully compared. To address this issue, for each data set we randomly selected four data points out of the whole set, and regressed over it using a power law. We selected this number of data points because it is the number of timescales from the data sets with least timescales that is still usable. We repeated the process 5,000 times, generated a distribution of powers, and computed the mean and median of all trials. As a result, we were left with 26 averaged powers ("four-terrace analysis"), which we used in the test described in section 2.3.

We determined whether each of the models yield a positive or a negative outcome to the model data sets using p-values derived from a Kolmogorov-Smirnov (KS) test, calculated between the model data sets and an artificial data set that incorporates terrace elevation noise (see section 2.3). A KS test examines the maximum vertical difference between an empirical distribution and a reference distribution. Our null hypothesis is the assumption that the distribution of averaged powers from the four-terrace analysis is equal to the distribution of artificial data—derived either for a linear or nonlinear process. For each KS test throughout this study we calculated an associated p-value, which gives the significance level at which the null hypothesis can be rejected. In many cases and depending on the field of study, the null hypothesis is rejected if the p-value <0.05.

2.3. Artificial Data Analysis (ADA)

We exploited ADA to evaluate the nature of the relationship between incision rate and timescale. Specifically, our ambition was to develop a statistical criterion for distinguishing whether or not the incision rates from the field data are dependent on timescale (Equation 7 vs. Equation 10). We applied the ADA with two key objectives: (a) to derive statistical confidence limits to establish a criterion to either accept or reject the linear model (Gallen et al., 2015) and (b) to test whether a single specific power law exponent is consistent with the field data. In this test, the absence of a clear solution indicates that the exponent is variable rather than constant (Schumer & Jerolmack, 2009). Below, we first describe the ADA approach for (a), before generalizing it to address (b).

We used the 26 powers, generated in the four-terrace analysis, to compare against 26 model powers, computed using ADA-derived elevation-timescale profiles (Figure 2). The derivation of the latter is described as follows. Consider a T_{tot} (kyr) history of a river bed subjected to a constant incision rate E [mm yr^{-1}]. During this period, N_{st} strath terraces are formed along a timeline with spacing of T_{tot}/N_{st}. The terraces are then assigned an elevation Z using the constant incision rate multiplied by the time that has passed until the terrace has formed. This is the underlying process that mimics an initially linear profile according to Equation 10 with an intercept $t_A = 0$ and a slope of E. A few further steps were taken in order to make the ADA comparable to the field data, which are described below.

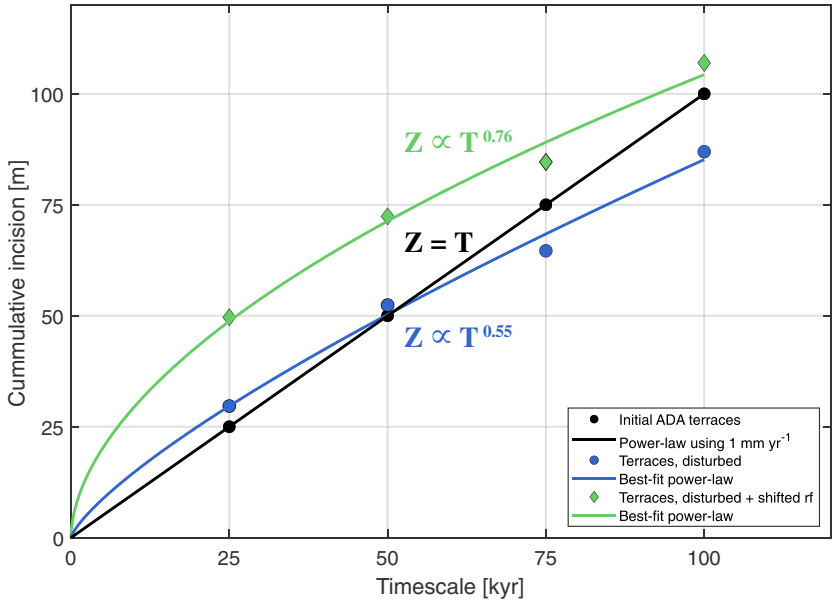

Figure 2. An example of the applied process in the linear artificial data analysis (ADA). First, four terraces were generated and were equally spaced in time, using a total time span of 100 kyr (black circles). Second, the terraces were randomly disturbed (blue circles) using a Gaussian noise function with a varying standard deviation error ϕ, which is set to 0.2 in this example. Third, an elevation bias was introduced by shifting the reference frame (rf; green diamonds), 20 m in this example. Finally, to each of the plotted group terraces, a power law regression was fitted, and the best fit exponents are shown in the figure. Prior to the disturbance, the exponent is 1 (black line). After the disturbance, there is a dependence on the timescale (exponent of 0.55; blue line), whereas the reference frame shift introduced a time dependency, resembled by an exponent of 0.76 (green line).

1. To be consistent with the field data powers (four-terrace analysis), we generated a sequence of $N_{st} = 4$ using a constant incision rate $E = 1$ and a total time span $T_{tot} = 100$, which resulted in terrace time spacing of $\frac{T_{tot}}{N_{st}} = 25$ (kyr).
2. To assess the variability of the modeled γ power, we then vertically translated each of the four terraces using a Gaussian Noise Function (GNF), that is, a normal distribution with a mean of 0 and a standard deviation equals to ϕZ, where ϕ is the error percentage, which was varied between 0 to 0.5 in the simulations.
3. We introduced a reference frame bias and shifted the whole profile accordingly. This process was produced simultaneously using two distinct distribution functions, each of which corresponds to a different mechanism:
   i. A normal distribution with a mean of 0 and a varying standard deviation STD_{norm}, (iterated 0 to 100 m). This allowed us to simulate a climatic cycle with delayed and accelerated incision phases, relative to a mean incision rate, according to Gallen et al. (2015).
   ii. An exponential distribution with varying mean μ_{exp} (iterated 0 to 100 m). This distribution yields only positive values and was intended to simulate a reference frame bias solely due to bed aggradation by sediments.
4. For each pair of ϕ and either STD_{norm}, or μ_{exp} (hereafter referred to as "parameter pairs"), a power law regression was applied and best fit parameters and the associated R^2 were recorded.
5. A KS test was utilized to test the 26 ADA-derived against the 26 field data-derived powers, and an associated p-value was computed.
6. The whole process (1–5) was repeated 1,000 times, resulting in $26 \times 1{,}000 = 26{,}000$ parameters (constant, power and R^2) and 1,000 p-values for each of the parameter pairs.
7. We calculated a mean of all powers, R^2 and p-values for each of the parameter pairs. To assess the extent in which the ADA produces powers that are consistent with the "Sadler effect," we also computed the fraction of powers <1.

We extended the approach described above to address aim (b) by replacing the linear relationship between terrace age and elevation with a nonlinear relationship, thus modeling an incision rate dependent on timescale using the ADA. Again, we simulated an incision history with the same T_{tot} and four terraces were generated. In contrast to the linear case, for each timescale we used Equation 2 to calculate the incision rate I, using an iterated exponent γ, which was varied between 0 and 2. Then, we used the calculated I to assign each terrace with an elevation using the relation $Z = IT$. Next, we shifted each terrace elevation using the GNF, based on different ϕ values, and we repeated this processes 1,000 times as in the linear case. In this analysis we did not shift the reference frame.

In order to make predictions for both the linear and the variable exponent power law models, and to compare the ADA to field data sets, we used the following constraint. For each of the parameter pair values during the model runs, we counted how many younger terraces result in a higher elevation position in comparison to older terraces. We refer to this configuration as "swapped terraces". Swapped terraces are deemed to be unphysical, because an older strath terrace at a lower elevation would need to be eroded to make the formation of a younger strath terrace at a higher elevation possible. We correlated the total number of swapped terraces, normalized by the total number of generated terraces, to ϕ (and also STD_{norm} and μ_{exp} in the case of the linear ADA).

2.4. Statistical-Empirical Evaluation of the Data Set

Using the whole global data set (34 data sets; Table 2), our goal was to determine whether we can construct a relationship between incision rate and timescale (e.g., Equation 2) for practical usage. Naturally, these data were collected from different regions and encompass a wide range of tectonic histories, climate and lithology. Because the timescale over which incision was measured spans numerous orders of magnitude, it cannot be expected that a single equation can adequately describe incision rate over the range of timescale variability. In other words, we do not expect that simply regressing incision rate versus timescale would yield a reliable equation with a high R^2. Accordingly, we adopted a statistical-binning approach. Bins of the independent variable were chosen, and the corresponding data of the dependent variable that were within a specific range, defined by the bin width, were captured and classified to correspond to the bin. There are several ways of choosing bin widths. To assess in how far the outcome of this analysis is dependent on the number of bins chosen and on their spacing, we performed a sensitivity analysis, in which we varied the number of bins from 4 to 25, and documented the outcome from regressions, as well as the R^2. We used log-spaced bins, because the alternative, linearly spaced bins, bias the statistics toward high incision rates. The global data were log-binned according to the timescale described above and percentiles of incision rate were calculated for each timescale bin in 5 percentile steps.

After the binning procedure, we sought a relationship between incision, timescale, and percentile. Using log-transformed data (Ferguson, 1986; Miller, 1984), we fitted Equation 2 between incision rate and timescale to each of the different percentiles and saved the corresponding parameters. Subsequently, we separately plotted a and $\gamma - 1$ against the percentiles to assess if they can be further fitted with a specific function.

3. Results

3.1. Global Compilation of Fluvial Incision Rates

The global analysis yielded 581 data points from 34 studies measured at 148 sites (Table 2), including some previous compilations, for example, Dethier (2001). The time over which incision rates are averaged ranges from several days to more than 20 million years (Figure 3a) with majority of the data between 10^3 and 10^7 yr. Measured incision rates I span 8 orders of magnitude, ranging from 0 to 8.8×10^5 mm yr^{-1} (Figure 3b), although the majority of the rates are between 10^{-2} and 10^2 mm yr^{-1}. Several of the exceptionally high incision rates (>1,000 mm yr^{-1}) represent single floods, when a few meters of rock were removed within days or weeks (e.g., Lamb & Fonstad, 2010). The average, standard deviation (std) and median incision rate values are 2,180, 3.8×10^4, and 0.34 mm yr^{-1}, respectively. The std value is 17 times larger than the average, which is ~6,380 times larger than the median, illustrating the large variability of the data (Figure 3b).

3.2. Field Data

In general, measurements over shorter timescales correspond to higher incision rates (Figure 4). However, for a given timescale, incision rate spans up to 5 orders of magnitude. Computed for 26 different published

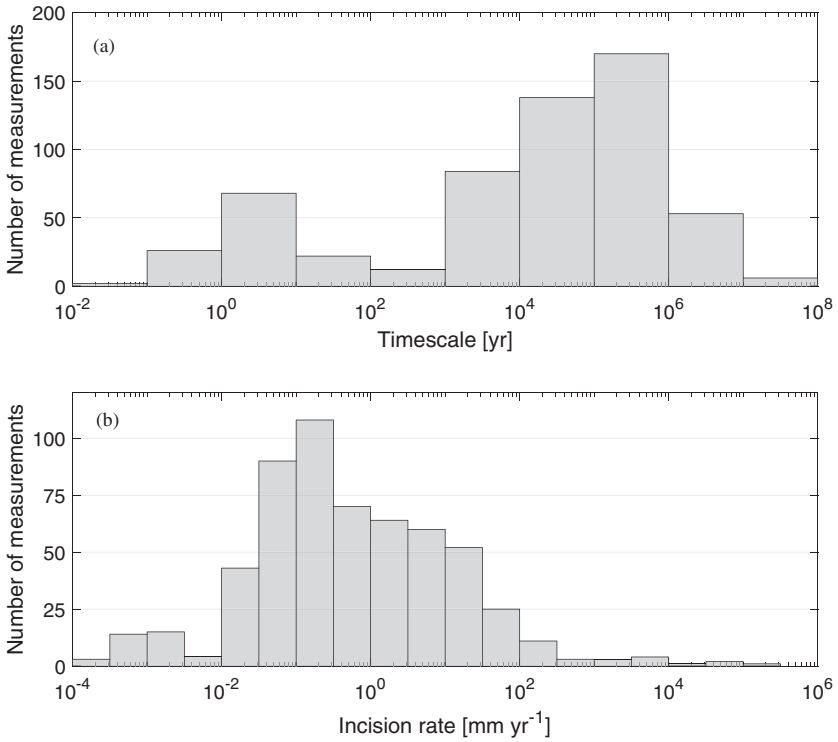

Figure 3. Histograms of the timescale (a) and observed incision rates (b) of the global data compilation ($N = 581$). Note the log scale for the horizontal axes.

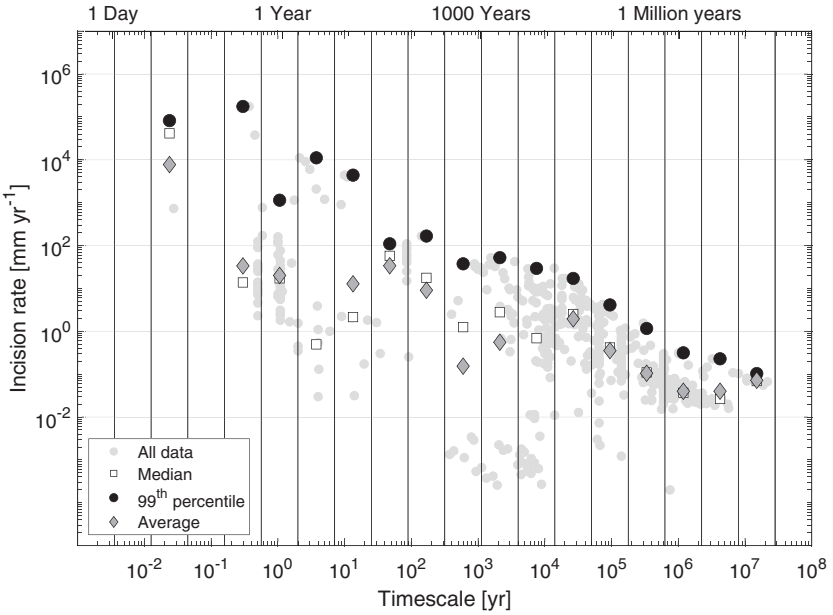

Figure 4. Incision rate (raw data, gray circles) versus timescale with vertical black lines are borders of the timescale bins. The data were classified into 21 bins using evenly log spaced bin widths, according to the time over which incision is averaged. For each time bin, the corresponding incision data were classified, and several statistics were calculated; see legend. The statistics were shifted in the horizontal direction toward the log-average location between each two neighboring bin borders for regression and appearance.

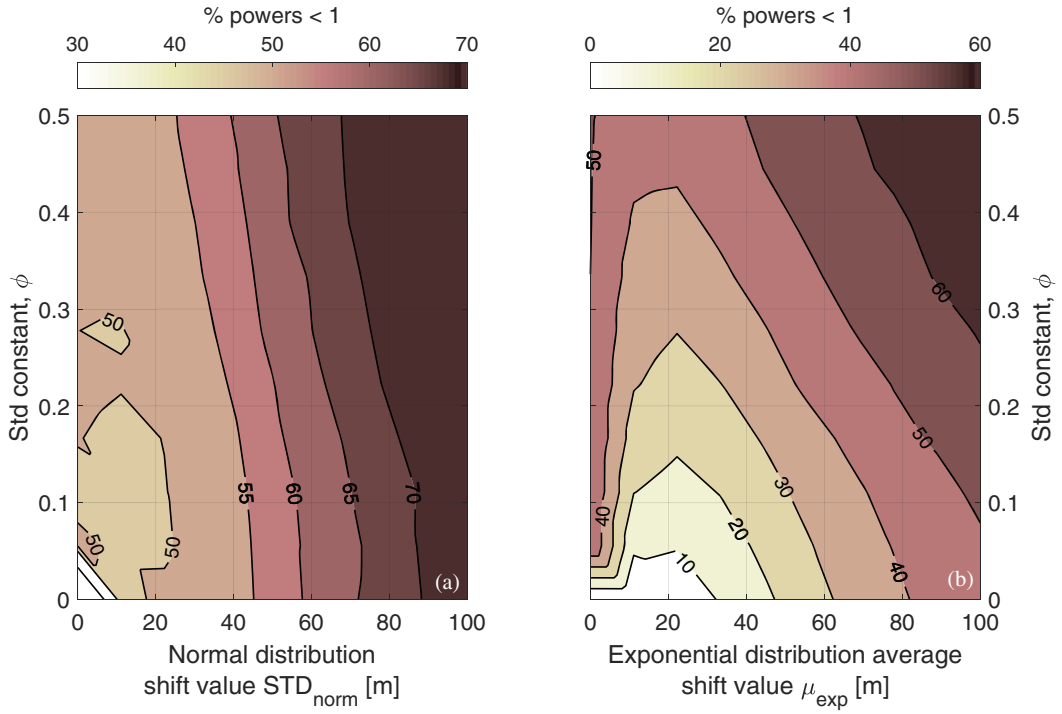

Figure 5. Tests of the linear model using the artificial data analysis. (a) A three-dimensional map depicting the fraction of powers smaller than 1, using a reference bias that is shifted using a normal distribution. The fraction is sensitive to the reference bias standard deviation STD_{norm} and is less sensitive to ϕ. (b) Same as in (a), only for the mean shift value of an exponential distribution. Note that the fraction of powers smaller than 1 is primarily sensitive to ϕ if μ_{exp} is low. Additionally, the fraction of powers smaller than 1 is never higher than ~60% and a range of 0% to 50% dominates almost entirely in the parameter pair space.

data sets, the exponent γ (Equation 1) ranges from −0.05 to 2.44 (Table 2), with an average and a std of 0.62 and 0.56, respectively, a R^2 range of 0.03 to 0.99, and an average R^2 of 0.53. Using fixed γ values of 0.5 and 0.25 (as in the models depicted in Table 1), the regressions yield average R^2 of 0.42 and 0.33, respectively (Table 2).

3.2.1. Testing the Linear Model Using Artificial Data

To test whether the data sets can be regarded as time independent, that is, terrace elevation scales linearly with timescale, we utilized the ADA described in section 2.3 (Figure 2). Using a reference frame bias controlled by a normal distribution (Figure 5a), the model predicts that the fraction of powers smaller than 1 ranges between ~40% and slightly above 70%. This range is almost entirely controlled by the standard deviation of the normal distribution shift, STD_{norm}, rather than the GNF constant of the standard deviation, ϕ (Figure 5a). Using an exponential distribution to simulate reference frame bias controlled by aggradation (Figure 5b), the fraction of powers smaller than 1 is dependent on both ϕ, and the mean value used in the exponential distribution, μ_{exp}. The largest amount of powers smaller than 1, 50%, is yielded in the model using $\phi > 0.3$ and $\mu_{exp} > 70$ m.

In the linear test, we divided the results between reference frame bias using (i) a normal distribution, and (ii) an exponential distribution. For (i), the p-values that were computed using the KS test between the distributions of ADA and field data exponents span the range of 0 to about 0.5 (Figure 6a) and are dominantly controlled by STD_{norm}. For low ϕ values (<0.1), the p-values increase from 0.01 to about 0.5 when STD_{norm} increases, respectively, from 35 to 85 m. The fraction of swapped terraces, which ranges from 0% to slightly above 20%, increases only with ϕ and is independent of STD_{norm} (Figure 6b). For ϕ of 0.1, there is a ~1% chance to obtain a swapped terrace.

For (ii), the p-values range from 0 to 0.05 and are both dependent on ϕ and μ_{exp} (Figure 7a). If the latter is smaller than 60 m, p-values increase with ϕ up to 0.05 for $\phi = 0.5$. If it is bigger than 60 m, than p-values increase toward large ϕ and μ_{exp}. The fraction of swapped terraces for the exponential distribution

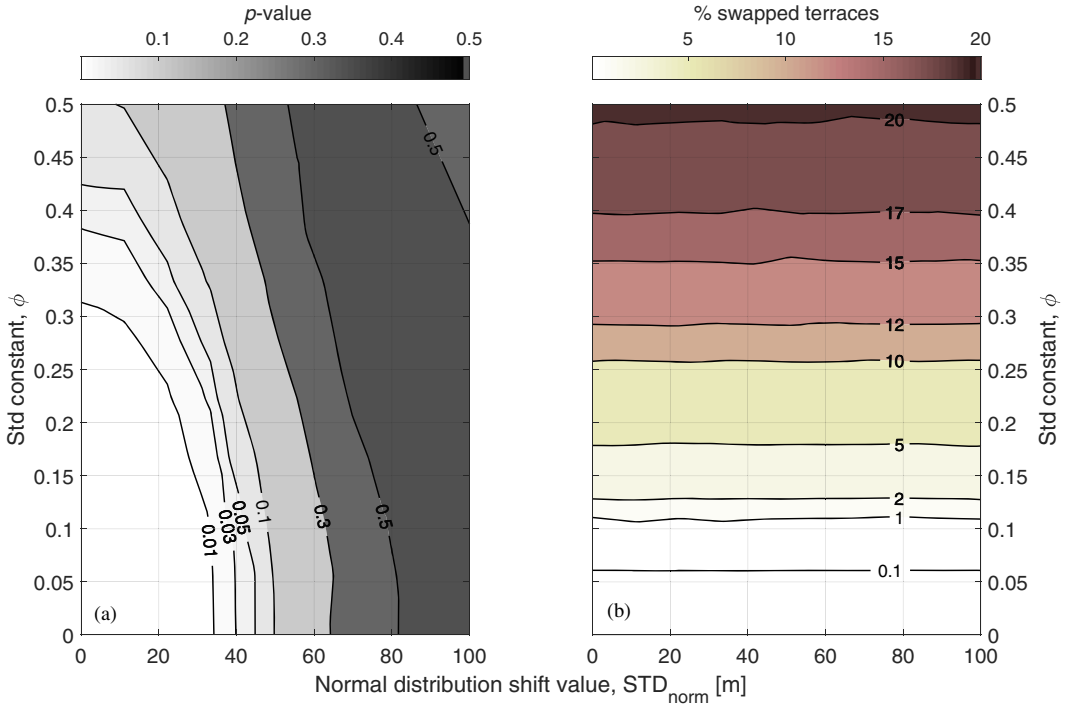

Figure 6. Linear model ADA test against model data sets ($N = 26$). (a) p-values, computed using a two-sided Kolmogorov-Smirnov test to the cumulative distributions of the empirical data sets and the distribution of power law-derived exponents, generated using the artificial data analysis with a reference frame bias controlled by a normal distribution. The p-values are higher than the significance level of 0.05 starting from a shift with $STD_{norm} > 45$ m or for high ϕ values. (b) The fraction of swapped terraces is entirely controlled by ϕ rather than by STD_{norm}. At ϕ of ~0.05 there is a 1/1,000 probability for a terrace to be swapped, and it increases up to 1/5 with larger ϕ values.

reference frame bias exhibit a similar trend as that of the normal distribution shift, and also solely depends on ϕ, rather than on μ_{exp} (Figure 7b).

3.2.2. Testing the Variable Exponent Power Law Model Using Artificial Data

Next, we tested whether the data can be regarded as nonlinear, that is, whether incision rate depends on timescale. In the ADA with nonlinear dependence of elevation on timescale, the highest fraction of swapped terraces, ranging from 0% to 35%, is observed for lower exponents and high ϕ values (Figure 8b). The computed p-values between the nonlinear ADA and the distribution of the global data sets γ increase from 0 to 0.5, create a valley-like shape, and are dependent on both ϕ and γ (Figure 8a). The highest p-values correspond to the median exponent of the global data sets, which is slightly above 0.5 and to ϕ values of above 0.3. For a significant results of p-value >0.05, and γ of ~0.5, ϕ needs to be 0.1 or higher (Figure 8a), which corresponds to 2–3% swapped terraces (Figure 8b).

3.3. Controls on γ and Empirical Relation Between Incision Rate, Timescale and Percentile

For several of the bins, there are only a few data points available, especially for the extreme incision rates. For example, there are two and seven data points in lowest and highest timescale bins, respectively. Using the evaluated γ values (Table 2) and general information on lithology and climate, we do not observe any systematic difference in γ with contrasting climatic and lithological classes (Figure 9). The sensitivity analysis shows that the regression parameters and R^2 are dependent on the number of chosen bins (Figure S2). The resulting power and coefficient of Equation 2 can be described with a negative linear ($R^2 = 0.97$) and an exponential model ($R^2 = 0.99$)—see Figure 10. The predicted incision rate, $I(T, P)$ with units of mm yr^{-1}, for percentile P (%) in a timescale T (yr) is given by

$$I(T, P) = 0.6\, e^{0.09P} T^{-(0.3172 + 0.0036\, P)} \quad (11)$$

The dependency of incision on T is a power function, whereas the dependency on P is exponential (Figure 10). However, the exponent in the timescale term is linearly dependent on the percentile as well.

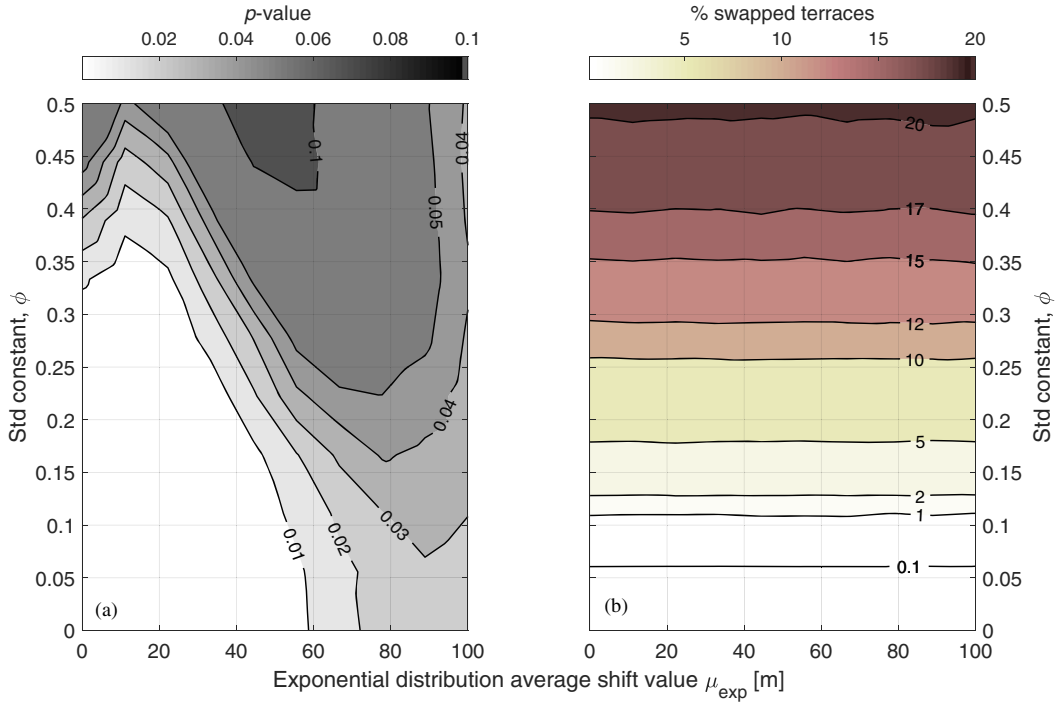

Figure 7. Linear model ADA test against model data sets ($N = 26$). (a) p-values, computed using a two-sided Kolmogorov-Smirnov test to the cumulative distributions of the empirical data sets and the exponent distribution generated using the artificial data analysis with a reference frame bias controlled by an exponential distribution. The p-values are higher than the significance level of 0.05 only if ϕ is larger than 0.25. (b) The fraction of swapped terraces shows a fairly similar tendency as in the case for a reference frame shifted using a normal distribution (Figure 6b).

Using Equation 11, the range of possible percentiles $0 \leq P_{\%} \leq 100$ depicts that $\gamma - 1$ lies between -0.32 and -0.70 (see Table S1 for the regression parameters and R^2 values). For the median, incision rate depends on timescale to a power of -0.51.

4. Discussion

4.1. Completeness and Bias of the Data Set

The collected data cover a broad range of field conditions and settings and should be largely representative for mountain streams located on the northern hemisphere. Measured incision rates, spanning 10 orders of magnitudes (Figure 3b), are a result of a variety of different methodologies related to obtaining ages of strath terraces and estimations of short-term incision rate. The data span the entire range of climatic regions, from cold over temperate and subtropical to tropical, with different types of climate forcing (e.g., monsoon climate, typhoons; Figure 9). Thus, in terms of climate, the data can be regarded as representative for the major climatic zones. Current information on climate, tectonic regime, location, and geomorphological parameters may not be representative for the entire time over which incision rates have been calculated, and for the specific times at which incision occurred.

The collected data are prone to two major biases. (i) A threshold-induced bias, which arises due to a minimum threshold incision rate that can be meaningfully recognized using a given measurement capability at a given timescale. For example, the method of Structure from Motion (SfM) performed using drone images of a Taiwanese bedrock river, yielded erosion detection uncertainties of up to ~30 cm (Cook, 2017). Assuming a steady incision rate of 1 mm/yr, in the course of 10 yr one would not be able to observe that erosion occurred, because only 1 cm of the bedrock was removed. In contrast, after 1,000 yr a total of 100 cm has already been eroded, and can be observed using the SfM with a minimal threshold of 30 cm. As a result, the minimum threshold incision rate that can be estimated with this particular method is decreasing with increasing timescale, from ~1.1×10^5 mm/yr over the course of a day to 300 mm/yr over 1 yr to 0.3 mm/yr over 1,000 yr, which would yield a power γ of 0. (ii) a selection bias that arises due to the

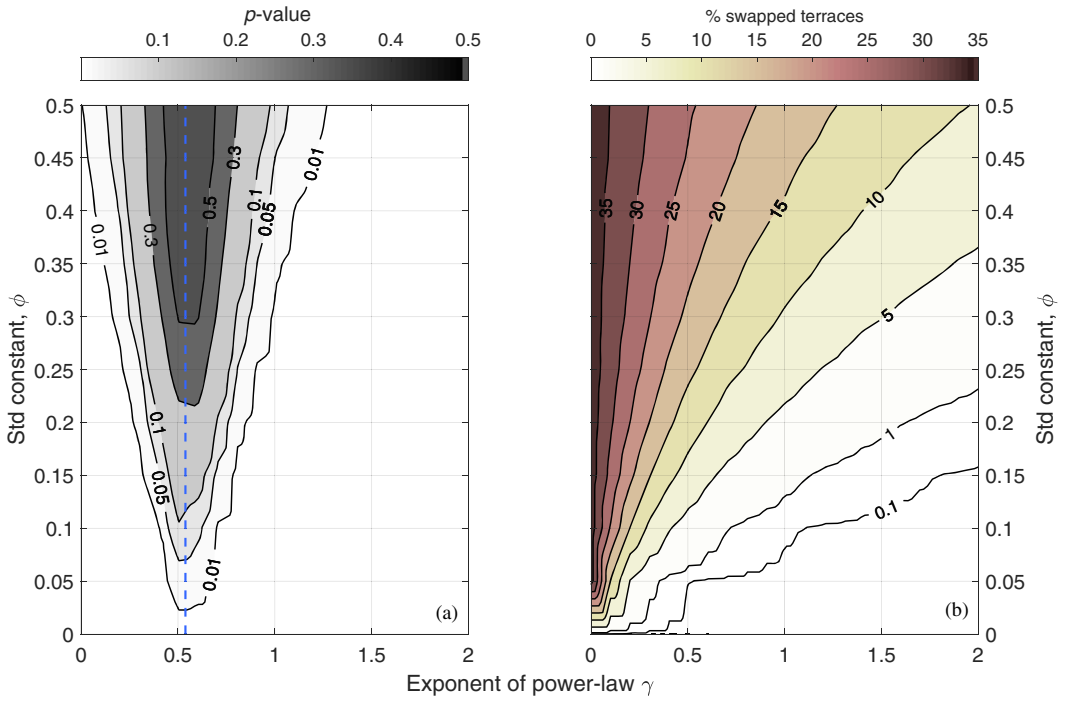

Figure 8. Nonlinear model ADA test against model data sets ($N = 26$). The x axis depicts the exponent of the power law imposed on the relationship between terrace elevation and timescale (Equation 1). (a) p-values, computed using a two-sided Kolmogorov-Smirnov test to the cumulative distributions of the empirical data sets and the exponent distribution generated using the artificial data analysis. Dashed blue line is the median of the field data exponents. The p-values are as high as 0.5, but only for large ϕ (>0.3) values, which necessitates a large fraction of swapped terraces (b). (b) The fraction of swapped terraces is sensitive both to ϕ and to the exponent γ. More terraces are swapped for lower γ and higher ϕ values.

tendency of researchers to study large impact or extreme events (e.g., Lamb & Fonstad, 2010) (see, for example, the data for ~10^{-2} yr in Figure 4). Both of these biases can be expected to be more important on short than on long timescales, yielding average incision rates larger than the unbiased rate. This means that the average incision rate for short timescales (days, months, years) (Figure 4) is larger than the actual unbiased rate. However, these sources of bias decrease with long-term timescales (>10^3 yr), because (1) rare floods may dominate long-term erosion and are more likely to occur (Kirchner et al., 2001), and (2) even in the case of an erosion close to 0, the division of a small number in a large timescale would yield a small incision rate, which is what we expect from the "Sadler effect" (Figure 4). Evidence for these biases is apparent in our data in the form of the dependence of the power γ on the percentile (Figure 10b). The power γ in the relationship between incision rate and timescale is steep for low percentiles ($\gamma = 0.62$ for $P = 5\%$), but gradually becomes lower with higher percentiles ($\gamma = 0.30$ for $P = 99\%$), which may indicate a systematic decrease in the biases toward high percentiles. For example, if for a given percentile, the biased average is always higher than the unbiased average, but this effect is systematically lesser for larger percentiles, then we can expect a decreasing relationship between γ and the percentile. Hence, if the data were not biased, we could have expected only an increase of the coefficient with the percentile (Figure 10a). Ultimately, the maximum observed incision rate I_{max} is not biased, and thus the 100th percentile of the data can be utilized as a nonbiased estimator, and is given by

$$I_{max} = 9177.6T^{-0.70} \quad (12)$$

With an associated R^2 of 0.94 (see Table S1 for errors on the evaluated parameters).

4.2. Evaluation of the Global Data Sets to Published Models

The fraction of powers smaller than unity is associated with the "Sadler effect," because the decrease of incision rate with timescale is only relevant for $0 \leq \gamma \leq 1$. If the standard deviation of the reference frame bias is

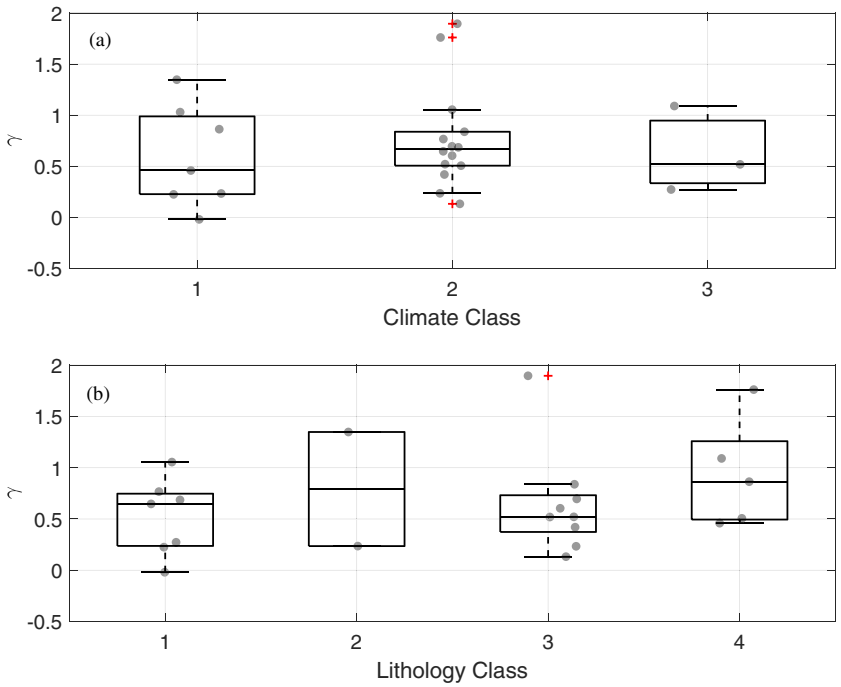

Figure 9. Boxplots of potential parameter control on γ. The x axes in (a) and (b) are classified groups of climate and lithology, respectively. (a) The power γ versus three different climate classes with the numbers 1, 2, and 3 corresponding to increasing extreme conditions, ranging from cold and dry (1) to extreme wet (e.g., Taiwan) in (3). (b) The power γ versus three different lithology classes, in general increasing strength from 1 (e.g., sandstone) to 4 (e.g., granites).

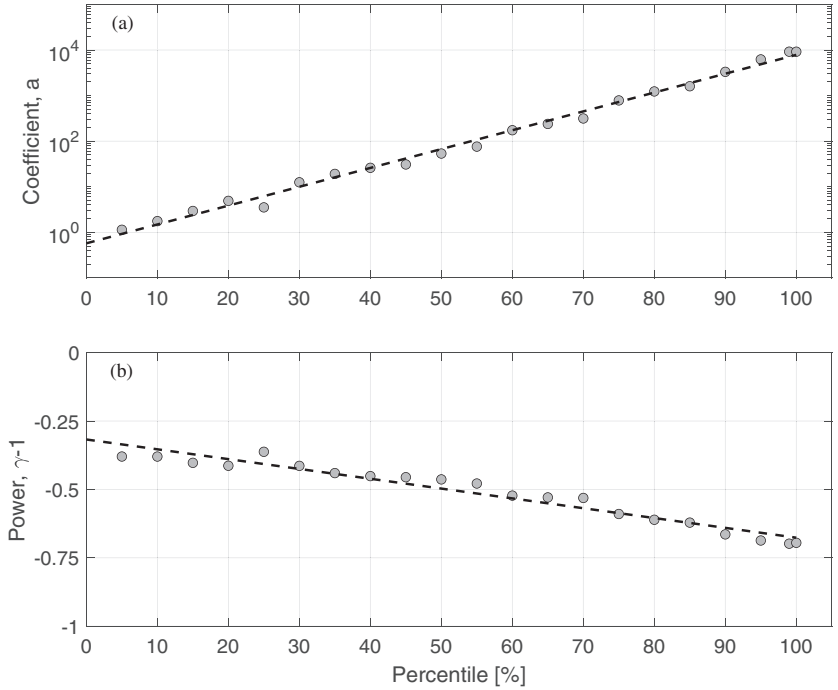

Figure 10. Best fit coefficient, a (a) and power, $\gamma - 1$ (b) of Equation 2 for the different percentiles of incision rate in Figure 4. The coefficient a increases exponentially [$a = (0.601 \pm 0.131)e^{(0.0944 \pm 0.00411)P_{\%}}$; $R^2 = 0.99$]. The power $\gamma - 1$ decreases linearly with the percentile ($\gamma - 1 = -(0.00356 \pm 0.000451)P - 0.317 \pm 0.0269$; $R^2 = 0.94$). Uncertainties are computed errors with 95% significance. See Table S1 for the regression parameters and associated R^2.

>10 m, the linear ADA predicts the "Sadler effect" to dominate over 50% of the trails, when the bias is normally distributed (Figure 5a). Even for low values, for example, ϕ of 0 and STD_{norm} of 15 m, the model predicts that 50% of the resultant powers are smaller than 1. This is not the case for the linear ADA with a reference frame bias that is controlled by an exponential distribution (Figure 5b). In this case, to predict at least 50% of the powers that are smaller than 1, STD_{norm} has to be larger than 40 m with a ϕ value of about 0.5, or alternatively ϕ value of 0.08 associated with STD_{norm} of 100 m. At this latter value of ϕ, there is a 0.1% chance to get a swapped terrace, that is, 1 out of 1,000 strath terraces is located above an older terrace. Even if it is possible to swap terraces (Schumm & Parker, 1973), it is very unlikely. For example, consider a bedrock river undercutting its bed and incising vertically downward. At a certain point in time, a strath terrace is abandoned while the river keeps incising downward. This terrace is the first one, thus the oldest. At a later stage, the river is filled with large amounts of sediment deposits and begins to grade, elevating its absolute bed elevation. In order for a younger terrace to be located above the oldest, the bed must be higher than the first terrace. While this is general plausible, the older terrace can be expected to be destroyed by fluvial processes. In addition, no swapped terraces were observed in any of our data sets. We hence rule out the possibility of a younger terrace to be located above an older terrace.

For a ϕ value that is associated with ~0 terrace swapped ($\phi <$ ~0.05), the computed p-values between the field data and the linear ADA using the normal distribution as a reference frame bias (Figure 6), indicate that a significant result (p-value >0.05) is possible in the parameter space if STD_{norm} is at least 45 m. Using the statistics that characterize a normal distribution, this latter value means that ~68% and ~31.5% of the data must have a retarded incision (relative to the averaged incision rate) or sediment aggradation elevations as high as 45 and 135 m, respectively. In Taiwan, one of the most active erosional locations on Earth, typhoons are known to deposit sediment with few meters of elevation above the bedrock (Lague, 2010). Massive aggradation is possible, but it seems implausible that at any time, around a third of all rivers show tens to hundreds of meters of sediment on their beds. A measurement can be potentially taken at a time when the actual river bed at that same time is located above the expected location of the bedrock using the long-term averaged incision rate. However, this situation necessitates a prolonged retarded incision phase. Feedbacks within the river system are expected to keep the river near a steady state in which both the imposed sediment load can be transported and where incision rate is equal to the baselevel lowering rate (Turowski, 2020). Retarded incision may occur locally, but creates elevated slopes with respect to the baselevel, which increases incision rates. As a result, bedrock elevations higher than the steady state level by tens of hundreds of meters seem implausible. It is for these reasons that we reject the linear model that incorporates a reference frame bias characterized by a normal distribution. As for the linear ADA with a reference frame bias that is characterized by an exponential distribution (Figure 7), the significant results of p-value >0.05 are only possible in association with at least ~10% of swapped terraces. Thus, this model can also be rejected.

The constant exponent power law models (Pelletier & Turcotte, 1997; Sadler & Strauss, 1990; Strauss & Sadler, 1989) (Table 1) yielded reasonable R^2 values, yet fixing the exponent to constant values of 0.25 and 0.5 yielded 11.5% and 23% data sets corresponding to a R^2 of 0, respectively (Table 2). The nonlinear ADA shows that a constant exponent power law model is not acceptable since a significant result is possible (Figure 8a) only in association with at least ~3–4% swapped terraces (Figure 8b). In general, higher p-values are obtained merely due to the flexibility of the GNF to alter vertical location of terraces in a wide elevation range. On this basis, the constant exponent power law models can be rejected as well.

In contrast to the constant exponent power law models, the variable exponent power law model (Schumer & Jerolmack, 2009) yielded higher R^2 values when fitted to the data (Table 2), but has one more degree of freedom. This may indicate that the higher R^2 values calculated for this model are simply a result of more freedom in the adjustment of the model parameters. Notwithstanding, the inability of the linear and constant power models to statistically characterize all 26 tested data sets, combined with the range of exponents yielded by a power law model (Equation 1), support a variable power. Indeed, the discrepancy between the nonlinear ADA and the distribution of data set exponents, represented by the median (Figure 8), could only be explained if the field data exponents were drawn from different underlying distributions. Therefore, our results suggest that the link between incision rate and timescale is statistically best explained by a nonlinear power law relation with a variable exponent γ in accordance with the model proposed by Schumer and Jerolmack (2009). These findings also support the argument of Ganti et al. (2016) for glaciated regions, that a

stochastic model better explains the "Sadler effect" because it requires a simpler premise, that is, a heavy-tailed hiatus distribution, whereas a deterministic model requires that erosion rates around the globe are remarkably higher in the present than in the past.

4.3. Controls on γ

With the establishment of a model with site-dependent γ, we now turn to discuss the potential controls on γ. From the field data, we obtained five values (19%) of $\gamma > 1$ while 21 values (81%) of γ were found to be smaller than 1. The former indicate an increase in incision rate with increasing timescale, while the latter indicate a decrease (Table 2). Values of γ larger than 1 also result in a negative instantaneous incision rate (I_{LT}; Equation 9), which is inconsistent with Schumer and Jerolmack's (2009) model (Figure S1). We suggest the following three potential reasons why γ values larger than 1 could arise. First, incision rates could have decreased if climate or tectonic forcing changed over the timescale over which incision is averaged, resulting in $\gamma > 1$. For example, a γ value of 1.1 was found for the Susquehanna River, where Reusser et al. (2006) reported incision rates averaged over a few cycles of changing climate. Similarly, a γ value of 2.44 was calculated for the southern Sierra Nevada, where G. M. Stock et al. (2005) discussed the possibility that bedrock incision pulse coincide in time with a Pleistocene tectonic event and a late Cenozoic climate change. Second, a systematic bias may arise due to the use of different methodology approaches. Specifically, if the age determination is systematically biased in different ways for different methods, and this bias happens to scale with time, then γ may be greater than 1. Finally, a value of $\gamma > 1$ may simply be a result of general uncertainty in the fitted power. Indeed, using a one-sample t-test statistic, three out of the five relevant data sets do not yield a power that is significantly different from 1.

For the range of values smaller than 1, γ is expected to reflect the range of incision hiatus length over the history of an eroded river. It is therefore expected to be controlled by forcing conditions. Specifically, we hypothesize that γ is controlled by tectonic events and a climatic regime that characterizes a particular field site over the timescale in question. For a given hiatus distribution, the probability for a long period without incision increases with decreasing γ values. Thus, for rivers undergoing incision phases during periods with similar length, the longest hiatus periods are expected for γ values that approach 0, and the shortest hiatus periods are expected for γ values that approach 1. There are three potential causes controlled by climate. First, through the occurrence of long drought periods, during which discharge is below the threshold for incision (Lague et al., 2005). Second, the variability in hiatus can be related to the variability in discharge, which is dependent on the variability in precipitation rates and the hydrologic regime (Deal et al., 2018). Bedload motion is necessary for incision, but it is a rare process that occurs generally only during floods. Contrary, large floods may deposit large amounts of sediment, inhibiting erosion for sustained periods during which the material is evacuated (e.g., Lague, 2010). Third, glaciation can also have a climatic effect on the distribution of incision hiatus. Glacial environments have been associated with prolonged periods of aggradation (Maizels, 1979), and melt water discharge allows for frequent sediment transport. In addition, proglacial lakes can trap sediment (Hicks et al., 1990), which may decrease the available amount of sediment in the river. Glacial lake outburst floods can alter the flood regime in a river and may be the geomorphically dominant events in some regions (Cook et al., 2018). Fourth, the occurrence of extreme storms that can trigger landslides that are able to block the channel (e.g., Korup et al., 2006). In this case, the channel is expected to be completely covered, thus inhibiting incision into bedrock. The occurrence of landslides dams has been shown to dominate landscape evolution (Ouimet et al., 2007) and to inhibit river incision for timescales of up to 10^4 yr (Korup et al., 2006). In the short term, landslides may impose upstream aggradation for sustained periods (Finnegan et al., 2019). Because earthquakes can also cause landslides, a similar mechanism allows for a tectonic control of the hiatus distribution.

In general, the main two parameters that are expected to influence the relationship between incision rate and timescale through the power γ are discharge variability and the threshold for erosion (Lague et al., 2005; Scherler et al., 2017). The former is expected to have an influence because low discharge variability imply greater discharges to be rarer in comparison to high discharge variability, given the same mean discharge. Then, flooding events with extensive sediment aggradation, followed by prolonged periods of degradation, may be rare. Since the size and shape of basins correlate with magnitude and duration of storms (Molnar et al., 2006), drainage area is also expected to influence γ through the dependency with discharge variability. The threshold for incision likely controls the probability of an incision event to occur, given specific

hydrometric conditions. For example, if the threshold is very high, incision is rare, and we expect extended hiatus periods. The power γ may also correlate with the frequency of and ground acceleration induced by earthquakes. It has been shown that γ values estimated for tectonically active regions are not statistically different from γ values estimated for inactive regions (Finnegan et al., 2014). Our finding that γ is not distinguishable using different classes of lithology and climate (Figure 9) does not rule out an effect of discharge variability. We hypothesize that, consequently, γ is expected to decrease toward 0 with increasing discharge variability, an increasing threshold for incision, and with decreasing drainage area.

4.4. Empirical Analysis

The empirical analysis yielded a relationship between incision rate, timescale and percentile (Equation 11). Although it is often argued that plotting a rate versus timescale yields a spurious correlation due to the time variable used to calculate the rate (Finnegan et al., 2014; Jerolmack & Sadler, 2007; Sadler et al., 1999), the results from the empirical model utilized from a rate regression are within regression errors of results yielded by a regression of incision length (Figure S2). The resultant model (Equation 11) can be utilized to evaluate the bias due to the "Sadler effect" introduced into comparisons of rates between different sites, or at the same site for measurements over different timescales. Importantly, the existence of the "Sadler effect" in bedrock incision data may mask true changes in incision rate over time. To robustly reveal these changes, the trends in incision rates due to the "Sadler effect" need to be removed, which can be accomplished using Equation 11. This may be relevant for several applications, including risk management and landscape change assessments. For example, the model can be used to assess the "Sadler effect" for conservative purposes, by using the 99^{th} percentile. In such a case, for example, a site-to-site comparison between terrace-derived rates that integrate contrasting ages of 10 and 500 kyr, would yield a bias of a factor of 15 solely due to a timescale dependence.

The goodness of the fit of Equation 11 (Figure 10) was determined using the coefficient of determination (R^2). Nonetheless, the R^2 of the relation between the exponent ($\gamma - 1$) and the percentile depends on the number of bins used for the regression (Figure S3). In our analysis, we showed the results for 16 log-spaced bins because (i) it yielded high R^2 and (ii) it gives higher time-resolution than other bins with high R^2 values. Using 13 bins rather than 16, for example, yields slightly higher R^2 for the power ($\gamma - 1$), 0.96 instead of 0.94, respectively, but the difference in the predicted coefficients are <5%, except for the constant of the exponential term (0.6 in Equation 11) which differs by ~20%. Furthermore, we observed increased R^2 values for the regression of Equation 11 with larger percentiles. For example, for the 5^{th}, 50^{th}, and 99^{th} percentiles, the associated R^2 were 0.37, 0.67 and 0.94, respectively (Table S1). This reinforces our expectation of a selection bias toward higher incision rates associated with extreme events.

The empirical data set comprising thousands of sediment accumulation estimates by Jerolmack and Sadler (2007) follows a break in the scaling relationship over timescale, with a crossover point that marks a transition between different γ values, which they interpreted to be a cause of a change in the dominant process. Such a crossover point is not observed in our data. In contrast, the median and average incision rate values (Figure 4) are scattered in the short-term timescales, while the trend shows less scatter in long-term timescales ($>10^4$ yr) and a stable trend of the 99^{th} percentile (R^2 of 0.94; Figure S3 and Table S1) along the entire timescale range.

5. Conclusions

We studied the dependence of incision rate on timescale for fluvial bedrock incision using a global data compilation from 34 papers. We examined three contrasting models that predict the scaling of incision rate with timescale: (i) the linear model (Gallen et al., 2015), (ii) the constant exponent power law model (Pelletier & Turcotte, 1997; Sadler & Strauss, 1990; Strauss & Sadler, 1989), and (iii) the variable exponent power law model (Schumer & Jerolmack, 2009). The linear and the constant exponent power law models were rejected on the basis of statistical criteria and because the observed scaling of incision rate with timescale using the field data sets is consistent with a variable exponent power law model. This means that incision rate is nonlinearly dependent on the time over which it is averaged, with a site-dependent scaling exponent. Most importantly, it implies that incision rates measured over different timescales cannot be meaningfully

compared without accounting for the Sadler effect. We propose an empirical equation considering the timescale and the percentile of the measured rate at a given timescale to address this issue.

Conflict of Interests

The authors declare that they have no competing interests.

Data Availability Statement

The raw data described in Table 2 can be found in the Zenodo data repository with the URL https://zenodo.org/record/3963718#.Xx_KYJ4zaUk (item https://doi.org/10.5281/zenodo.3963718).

Two MATLAB functions (linearFunc.m and nonlinearFunc.m) that were used to generate Figures 5–8 are available in the Zenodo data repository with the URL https://zenodo.org/record/3953416#.XxacY54zaUk (item https://doi.org/10.5281/zenodo.3953416).

Acknowledgments

We thank Liran Goren, Angela Landgraf, and Jonathan Laronne for providing detailed comments on an earlier version of the manuscript. The latter is thanked for introducing us to the work of Joseph Barrell. Reviews by Associate Editor Jon Pelletier, Editor Amy East, and two anonymous referees greatly improved the paper. This research was funded by the National Cooperative for the Disposal of Radioactive Waste (NAGRA), Switzerland. Ron Nativ is supported by the Ben-Gurion University of the Negev "high-tech, bio-tech and chemo-teck" scholarship and the Israel Science Foundation (grant No. 562/19). Open access funding enabled and organized by Projekt DEAL.

References

Anthony, M. D., & Granger, D. E. (2004). A late tertiary origin for multilevel caves along the western escarpment of the Cumberland Plateau, Tennessee and Kentucky, established by cosmogenic ^{26}Al and ^{10}Be. *Journal of Cave and Karst Studies*, 46–55.

Antón, L., Rodés, A., De Vicente, G., Pallàs, R., Garcia-Castellanos, D., Stuart, F. M., et al. (2012). Quantification of fluvial incision in the Duero Basin (NW Iberia) from longitudinal profile analysis and terrestrial cosmogenic nuclide concentrations. *Geomorphology*, *165–166*, 50–61. https://doi.org/10.1016/j.geomorph.2011.12.036

Barrell, J. (1917). Rhythms and the measurements of geologic time. *Bulletin of the Geological Society of America*, *28*(1), 745–904. https://doi.org/10.1130/GSAB-28-745

Beer, A. R., Turowski, J. M., & Kirchner, J. W. (2017). Spatial patterns of erosion in a bedrock gorge. *Journal of Geophysical Research: Earth Surface*, *122*, 191–214. https://doi.org/10.1002/2016JF003850

Brocard, G. Y., van der Beek, P. A., Bourlès, D. L., Siame, L. L., & Mugnier, J. L. (2003). Long-term fluvial incision rates and post-glacial river relaxation time in the French Western Alps from ^{10}Be dating of alluvial terraces with assessment of inheritance, soil development and wind ablation effects. *Earth and Planetary Science Letters*, *209*(1–2), 197–214. https://doi.org/10.1016/S0012-821X(03)00031-1

Burbank, D. W., Leland, J., Fielding, E., Anderson, R. S., Brozovic, N., Reid, R. M., & Duncan, C. (1996). Bedrock incision, rock uplift and threshold hillslopes in the northeastern Himalayas. *Nature*, *379*(6565), 505–510. https://doi.org/10.1038/379505a0

Cheng, S., Deng, Q., Zhou, S., & Yang, G. (2002). Strath terraces of Jinshaan Canyon, Yellow River, and Quaternary tectonic movements of the Ordos Plateau, North China. *Terra Nova*, *14*(4), 215–224. https://doi.org/10.1046/j.1365-3121.2002.00350.x

Cook, K. L. (2017). An evaluation of the effectiveness of low-cost UAVs and structure from motion for geomorphic change detection. *Geomorphology*, *278*, 195–208. https://doi.org/10.1016/j.geomorph.2016.11.009

Cook, K. L., Andermann, C., Gimbert, F., Adhikari, B. R., & Hovius, N. (2018). Glacial lake outburst floods as drivers of fluvial erosion in the Himalaya. *Science*, *362*(6410), 53–57. https://doi.org/10.1126/science.aat4981

Cook, K. L., Turowski, J. M., & Hovius, N. (2013). A demonstration of the importance of bedload transport for fluvial bedrock erosion and knickpoint propagation. *Earth Surface Processes and Landforms*, *38*(7), 683–695. https://doi.org/10.1002/esp.3313

Cook, K. L., Whipple, K. X., Heimsath, A. M., & Hanks, T. C. (2009). Rapid incision of the Colorado River in Glen Canyon—Insights from channel profiles, local incision rates, and modeling of lithologic controls. *Earth Surface Processes and Landforms*, *34*, 994–1010. https://doi.org/10.1002/esp.1790

Craddock, W. H., Kirby, E., Harkins, N. W., Zhang, H., Shi, X., & Liu, J. (2010). Rapid fluvial incision along the Yellow River during headward basin integration. *Nature Geoscience*, *3*(3), 209–213. https://doi.org/10.1038/ngeo777

Crow, R., Karlstrom, K., Darling, A., Crossey, L., Polyak, V., Granger, D., et al. (2014). Steady incision of Grand Canyon at the million year timeframe: A case for mantle-driven differential uplift. *Earth and Planetary Science Letters*, *397*, 159–173. https://doi.org/10.1016/j.epsl.2014.04.020

Cyr, A. J., & Granger, D. E. (2008). Dynamic equilibrium among erosion, river incision, and coastal uplift in the northern and central Apennines, Italy. *Geology*, *36*(2), 103–106. https://doi.org/10.1130/G24003A.1

Deal, E., Braun, J., & Botter, G. (2018). Understanding the role of rainfall and hydrology in determining fluvial erosion efficiency. *Journal of Geophysical Research: Earth Surface*, *123*, 744–778. https://doi.org/10.1002/2017JF004393

Dethier, D. P. (2001). Pleistocene incision rates in the western United States calibrated using Lava Creek B tephra. *Geology*, *29*(9), 783–786. https://doi.org/10.1130/0091-7613(2001)029<0783:PIRITW>2.0.CO;2

DiBiase, R. A., Whipple, K. X., Heimsath, A. M., & Ouimet, W. B. (2010). Landscape form and millennial erosion rates in the San Gabriel Mountains, CA. *Earth and Planetary Science Letters*, *289*(1–2), 134–144. https://doi.org/10.1016/j.epsl.2009.10.036

Dortch, J. M., Dietsch, C., Owen, L. A., Caffee, M. W., & Ruppert, K. (2011). Episodic fluvial incision of rivers and rock uplift in the Himalaya and Transhimalaya. *Journal of the Geological Society*, *168*(3), 783–804. https://doi.org/10.1144/0016-76492009-158

Duvall, A., Burbank, D., & Kirby, E. (2004). Tectonic and lithologic controls on bedrock channel profiles and processes in coastal California. *Journal of Geophysical Research*, *109*, F03002. https://doi.org/10.1029/2003JF000086

Ferguson, R. I. (1986). River loads underestimated by rating curves. *Water Resources Research*, *22*(1), 74–76. https://doi.org/10.1029/WR022i001p00074

Ferrier, K. L., Huppert, K. L., & Perron, J. T. (2013). Climatic control of bedrock river incision. *Letters to Nature*, *496*, 206–209. https://doi.org/10.1038/nature11982

Finnegan, N. J., Broudy, K. N., Nereson, A. L., Roering, J. J., Handwerger, A. L., & Bennett, G. (2019). River channel width controls blocking by slow-moving landslides in California's Franciscan mélange. *Earth Surface Dynamics*, *7*(3), 879–894. https://doi.org/10.5194/esurf-7-879-2019

Finnegan, N. J., Schumer, R., & Finnegan, S. (2014). A signature of transience in bedrock river incision rates over timescales of 10^4–10^7 years. *Letters to Nature*, *505*(7483), 391–394. https://doi.org/10.1038/nature12913

Gallen, S. F., Pazzaglia, F. J., Wegmann, K. W., Pederson, J. L., & Gardner, T. W. (2015). The dynamic reference frame of rivers and apparent transience in incision rates. *Geology*, *43*(7), 623–626. https://doi.org/10.1130/G36692.1

Gani, N. D. S., Gani, M. R., & Abdelsalam, M. G. (2007). Blue Nile incision on the Ethiopian Plateau: Pulsed plateau growth, Pliocene uplift, and hominin evolution. *GSA Today*, *17*(9), 4–11. https://doi.org/10.1130/GSAT01709A.1

Ganti, V., Von Hagke, C., Scherler, D., Lamb, M. P., Fischer, W. W., & Avouac, J. P. (2016). Time scale bias in erosion rates of glaciated landscapes. *Science Advances*, *2*(10), e1600204. https://doi.org/10.1126/sciadv.1600204

Gardner, T. W., Jorgensen, D. W., Shuman, C., & Lemieux, C. R. (1987). Geomorphic and tectonic process rates: Effects of measured time interval. *Geology*, *15*, 259–261. https://doi.org/10.1130/0091-7613(1987)15<259:GATPRE>2.0.CO;2

Granger, D. E., Fabel, D., & Palmer, A. N. (2001). Pliocene-Pleistocene incision of the Green River, Kentucky, determined from radioactive decay of cosmogenic ^{26}Al and ^{10}Be in Mammoth Cave sediments. *Bulletin of the Geological Society of America*, *113*, 825–836. https://doi.org/10.1130/0016-7606(2001)113<0825:PPIOTG>2.0.CO;2

Harel, M., Mudd, S. M., & Attal, M. (2016). Geomorphology global analysis of the stream power law parameters based on worldwide Be denudation rates. *Geomorphology*, *268*, 184–196. https://doi.org/10.1016/j.geomorph.2016.05.035

Harkins, N., Kirby, E., Heimsath, A., Robinson, R., & Reiser, U. (2007). Transient fluvial incision in the headwaters of the Yellow River, northeastern Tibet, China. *Journal of Geophysical Research*, *112*, F03S04. https://doi.org/10.1029/2006JF000570

Hartshorn, K., Hovius, N., Dade, W. B., & Slingerland, R. L. (2002). Climate-driven bedrock incision in an active mountain belt. *Science*, *297*(5589), 2036–2038. https://doi.org/10.1126/science.1075078

Hicks, D. M., McSaveney, M. J., & Chinn, T. J. H. (1990). Sedimentation in proglacial Ivory Lake, Southern Alps, New Zealand. *Arctic and Alpine Research*, *22*(1), 26–42. https://doi.org/10.2307/1551718

Jerolmack, D. J., & Sadler, P. (2007). Transience and persistence in the depositional record of continental margins. *Journal of Geophysical Research*, *112*, F03S13. https://doi.org/10.1029/2006JF000555

Johnson, J. P. L., Whipple, K. X., & Sklar, L. S. (2010). Contrasting bedrock incision rates from snowmelt and flash floods in the Henry Mountains, Utah. *Bulletin of the Geological Society of America*, *122*(9–10), 1600–1615. https://doi.org/10.1130/B30126.1

Karlstrom, K. E., Crow, R. S., Peters, L., McIntosh, W., Raucci, J., Crossey, L. J., et al. (2007). ^{40}Ar/^{39}Ar and field studies of Quaternary basalts in Grand Canyon and model for carving Grand Canyon: Quantifying the interaction of river incision and normal faulting across the western edge of the Colorado Plateau. *Bulletin of the Geological Society of America*, *119*, 1283–1312. https://doi.org/10.1130/0016-7606(2007)119%5B1283:AAFSOQ%5D2.0.CO;2

Kirchner, J. W., Finkel, R. C., Riebe, C. S., Granger, D. E., Clayton, J. L., King, J. G., & Megahan, W. F. (2001). Mountain erosion over 10 yr, 10 k.y., and 10 m.y. time scales. *Geology*, *29*, 591–594. https://doi.org/10.1130/0091-7613(2001)029%3C0591:MEOYKY%3E2.0.CO;2

Korup, O., Strom, A. L., & Weidinger, J. T. (2006). Fluvial response to large rock-slope failures: Examples from the Himalayas, the Tien Shan, and the Southern Alps in New Zealand. *Geomorphology*, *78*(1–2), 3–21. https://doi.org/10.1016/j.geomorph.2006.01.020

Lague, D. (2010). Reduction of long-term bedrock incision efficiency by short-term alluvial cover intermittency. *Journal of Geophysical Research*, *115*, F02011. https://doi.org/10.1029/2008JF001210

Lague, D., Hovius, N., & Davy, P. (2005). Discharge, discharge variability, and the bedrock channel profile. *Journal of Geophysical Research*, *110*, F04006. https://doi.org/10.1029/2004JF000259

Lamb, M. P., & Fonstad, M. A. (2010). Rapid formation of a modern bedrock canyon by a single flood event. *Nature Geoscience*, *3*(7), 477–481. https://doi.org/10.1038/ngeo894

Leland, J., Reid, M. R., Burbank, D. W., Finkel, R., & Caffee, M. (1998). Incision and differential bedrock uplift along the Indus River near Nanga Parbat, Pakistan Himalaya, from ^{10}Be and ^{26}Al exposure age dating of bedrock straths. *Earth and Planetary Science Letters*, *154*(1–4), 93–107. https://doi.org/10.1016/S0012-821X(97)00171-4

Litchfield, N., & Berryman, K. (2006). Relations between postglacial fluvial incision rates and uplift rates in the North Island, New Zealand. *Journal of Geophysical Research*, *111*, F02007. https://doi.org/10.1029/2005JF000374

Maizels, J. (1979). Proglacial aggradation and changes in braided channel patterns during a period of glacier advance: An alpine example. *Geografiska Annaler, Series A*, *61*, 87–101. https://doi.org/10.1080/04353676.1979.11879984

Metzler, R., & Klafter, J. (2000). The random walk's guide to anomalous diffusion: A fractional dynamics approach. *Physics Reports*, *339*(1), 1–77. https://doi.org/10.1016/S0370-1573(00)00070-3

Miller, D. M. (1984). Reducing transformation bias in curve fitting. *American Statistician*, *38*(2), 124–126. https://doi.org/10.1080/00031305.1984.10483180

Mills, H. H. (2000). Apparent increasing rates of stream incision in the eastern United States during the late Cenozoic. *Geology*, *28*(10), 955–957. https://doi.org/10.1130/0091-7613(2000)028<0955:AIROSI>2.3.CO;2

Molnar, P., Anderson, R. S., Kier, G., & Rose, J. (2006). Relationships among probability distributions of stream discharges in floods, climate, bed load transport, and river incision. *Journal of Geophysical Research*, *111*, F02001. https://doi.org/10.1029/2005JF000310

Molnar, P., & England, P. (1990). Late Cenozoic uplift of mountain ranges and global climate change: Chicken or egg? *Nature*, *346*(6279), 29–34. https://doi.org/10.1038/346029a0

Ouimet, W. B., Whipple, K. X., Royden, L. H., Sun, Z., & Chen, Z. (2007). The influence of large landslides on river incision in a transient landscape: Eastern margin of the Tibetan Plateau (Sichuan, China). *Bulletin of the Geological Society of America*, *119*, 1462–1476. https://doi.org/10.1130/B26136.1

Pazzaglia, F. J., & Brandon, M. T. (2001). A fluvial record of long-term steady-state uplift and erosion across the Cascadia forearc high, western Washington state. *American Journal of Science*, *301*(4–5), 385–431. https://doi.org/10.2475/ajs.301.4-5.385

Pelletier, J. D. (2007). Cantor set model of eolian dust deposits on desert alluvial fan terraces. *Geology*, *35*(5), 439–442. https://doi.org/10.1130/G23367A.1

Pelletier, J. D., & Turcotte, D. L. (1997). Synthetic stratigraphy with a stochastic diffusion model of fluvial sedimentation. *Journal of Sedimentary Research, Section B: Stratigraphy and Global Studies*, *67*, 1060–1067. https://doi.org/10.1306/d42686c6-2b26-11d7-8648000102c1865d

Personius, S. F. (1995). Late Quaternary stream incision and uplift in the forearc of the Cascadia subduction zone, western Oregon. *Journal of Geophysical Research*, *100*, 20,193–20,210. https://doi.org/10.1029/95JB01684

Plotnick, R. E. (1986). A fractal model for the distribution of stratigraphic hiatuses. *Journal of Geology*, *94*, 885–890. https://doi.org/10.1086/629094

Reusser, L., Bierman, P., Pavich, M., Larsen, J., & Finkel, R. (2006). An episode of rapid bedrock channel incision during the last glacial cycle, measured with ^{10}Be. *American Journal of Science*, *306*(2), 69–102. https://doi.org/10.2475/ajs.306.2.69

Reusser, L. J., Bierman, P. R., Pavich, M. J., Zen, E., Larsen, J., & Finkel, R. (2004). Rapid Late Pleistocene incision of Atlantic passive-margin river gorges. *Science*, *305*(5683), 499–502. https://doi.org/10.1126/science.1097780

Sadler, P. M. (1981). Sediment accumulation rates and the completeness of stratigraphic sections. *Journal of Geology*, *89*, 569–584. https://doi.org/10.1086/628623

Sadler, P. M., Bruns, P., & Haas, H. C. (1999). The influence of hiatuses on sediment accumulation rates on the determination of sediment accumulation rates edited by. *GeoResearch Forum*, *5*, 15–40. https://earthscience.ucr.edu/docs/Sadler_1999TransTech.pdf

Sadler, P. M., & Strauss, D. J. (1990). Estimation of completeness of stratigraphical sections using empirical data and theoretical models. *Journal of the Geological Society of London*, *147*(3), 471–485. https://doi.org/10.1144/gsjgs.147.3.0471

Schaller, M., Hovius, N., Willett, S. D., Ivy-Ochs, S., Synal, H. A., & Chen, M. C. (2005). Fluvial bedrock incision in the active mountain belt of Taiwan from in situ-produced cosmogenic nuclides. *Earth Surface Processes and Landforms*, *30*(8), 955–971. https://doi.org/10.1002/esp.1256

Scherler, D., Dibiase, R. A., Fisher, G. B., & Avouac, J. (2017). Testing monsoonal controls on bedrock river incision in the Himalaya and eastern Tibet with a stochastic-threshold stream power model. *Journal of Geophysical Research: Earth Surface*, *122*, 1389–1429. https://doi.org/10.1002/2016JF004011

Schumer, R., & Jerolmack, D. J. (2009). Real and apparent changes in sediment deposition rates through time. *Journal of Geophysical Research*, *114*, F00A06. https://doi.org/10.1029/2009JF001266

Schumm, S. A., & Parker, R. S. (1973). Implications of complex response of drainage systems for Quaternary alluvial stratigraphy. *Nature Physical Science*, *243*(128), 99–100. https://doi.org/10.1038/physci243099a0

Seong, Y. B., Owen, L. A., Bishop, M. P., Bush, A., Clendon, P., Copland, L., et al. (2008). Rates of fluvial bedrock incision within an actively uplifting orogen: Central Karakoram Mountains, northern Pakistan. *Geomorphology*, *97*(3–4), 274–286. https://doi.org/10.1016/j.geomorph.2007.08.011

Stock, G. M., Anderson, R. S., & Finkel, R. C. (2005). Rates of erosion and topographic evolution of the Sierra Nevada, California, inferred from cosmogenic ^{26}Al and ^{10}Be concentrations. *Earth Surface Processes and Landforms*, *30*(8), 985–1006. https://doi.org/10.1002/esp.1258

Stock, J. D., Montgomery, D. R., Collins, B. D., Dietrich, W. E., & Sklar, L. (2005). Field measurements of incision rates following bedrock exposure: Implications for process controls on the long profiles of valleys cut by rivers and debris flows. *Bulletin of the Geological Society of America*, *117*(1), 174–194. https://doi.org/10.1130/B25560.1

Strauss, D., & Sadler, P. M. (1989). Stochastic models for the completeness of stratigraphic sections. *Mathematical Geology*, *21*(1), 37–59. https://doi.org/10.1007/BF00897239

Turowski, J. M. (2020). Mass balance, grade, and adjustment timescales in bedrock channels. *Earth Surface Dynamics*, *8*(1), 103–122. https://doi.org/10.5194/esurf-2019-47

Turowski, J. M., & Cook, K. L. (2017). Field techniques for measuring bedrock erosion and denudation. *Earth Surface Processes and Landforms*, *42*(1), 109–127. https://doi.org/10.1002/esp.4007

Turowski, J. M., Hovius, N., Lague, D., Hsieh, M.-L., & Chen, M.-C. (2008). Distribution of erosion across bedrock channels. *Earth Surface Processes and Landforms*, *33*(3), 353–363. https://doi.org/10.1002/esp.1559

Wegmann, K. W., & Pazzaglia, F. J. (2002). Holocene strath terraces, climate change, and active tectonics: The Clearwater River basin, Olympic Peninsula, Washington State. *Bulletin of the Geological Society of America*, *114*(6), 731–744. https://doi.org/10.1130/0016-7606(2002)114<0731:HSTCCA>2.0.CO;2

Wegmann, K. W., & Pazzaglia, F. J. (2009). Late Quaternary fluvial terraces of the Romagna and Marche Apennines, Italy: Climatic, lithologic, and tectonic controls on terrace genesis in an active orogen. *Quaternary Science Reviews*, *28*(1–2), 137–165. https://doi.org/10.1016/j.quascirev.2008.10.006

Whipple, K. X. (2004). Bedrock rivers and the geomorphology of active orogens. *Annual Review of Earth and Planetary Sciences*, *32*(1), 151–185. https://doi.org/10.1146/annurev.earth.32.101802.120356

Whipple, K. X., Dollenmayer, K., & Snyder, N. P. (2000). Rates and processes of bedrock channel incision along the Upper Ukak River, Valley of Ten Thousand Smokes, Alaska. *Geology*, *28*, 835–838.

Willenbring, J. K., & Jerolmack, D. J. (2016). The null hypothesis: Globally steady rates of erosion, weathering fluxes and shelf sediment accumulation during Late Cenozoic mountain uplift and glaciation. *Terra Nova*, *28*(1), 11–18. https://doi.org/10.1111/ter.12185

Willenbring, J. K., & Von Blanckenburg, F. (2010). Long-term stability of global erosion rates and weathering during late-Cenozoic cooling. *Letters to Nature*, *465*(7295), 211–214. https://doi.org/10.1038/nature09044

Wobus, C., Whipple, K. X., Kirby, E., Snyder, N., Johnson, J., Spyropolou, K., et al. (2006). Tectonics from topography: Procedures, promise, and pitfalls. *Geological Society of America Special Paper*, *398*, 55–74. https://doi.org/10.1130/2006.2398(04)

Yanites, B. J., Tucker, G. E., Mueller, K. J., Chen, Y. G., Wilcox, T., Huang, S. Y., & Shi, K. W. (2010). Incision and channel morphology across active structures along the Peikang River, central Taiwan: Implications for the importance of channel width. *Bulletin of the Geological Society of America*, *122*(7–8), 1192–1208. https://doi.org/10.1130/B30035.1